

Second harmonic generation of TEA CO₂ laser radiation in LiInSe₂

Yu.M. Andreev,¹ V.V. Badikov,² P.P. Geiko,¹ S.G. Grechin,³ V.V. Efimenko,²
T.D. Efimenko,² V.L. Panyutin,² A.A. Tikhomirov,¹ and A.V. Shaiduko¹

¹*Institute of Optical Monitoring,
Siberian Branch of the Russian Academy of Sciences, Tomsk*

²*Kuban State University, Krasnodar*

³*Institute of Radioelectronics and Laser Technologies, Moscow*

Received January 13, 2004

The optical properties, damage threshold, and thermal conductivity of a new nonlinear LiInSe₂ crystal of the mm2 point symmetry group have been investigated. The transparency range of a red colored crystal is 0.4–13.5 μm at the zero level. The damage level is 248 ± 16 MW/cm² at 30 ns pulsed TEA CO₂ laser pump, that is, 1.7 times as high as that of ZnGeP₂. The thermal conductivity is 0.014 ± 0.002 W/cm² · K. Second harmonic generation was obtained for the first time for the TEA CO₂ laser. The energy conversion efficiency for the 9.55 μm emission line was 1.5% in energy and 2.6% in peak power at the pump intensity of 38.5 MW/cm², and that for the 9.26 μm line was 4.3% in peak power. The second harmonic generation efficiency versus the pump angle and wavelength is presented.

Introduction

Nonlinear crystals transparent in the visible, near IR, and mid IR regions, at least, up to 12–14 μm and having high birefringence are attractive owing to some reasons. Such crystals allow creation of fully solid-state sources operating in the mid IR, for example, tunable parametric light oscillators and difference frequency generators pumped by the Nd:YAG laser (wavelength of 1.06 μm) or the femtosecond Ti:sapphire (0.7–1.1 μm) and Cr:forsterite- (1.25–1.32 μm) lasers. With the use of the frequency converters into the UV and visible spectral regions available, it becomes possible to create fully solid-state sources operating in the region from 0.2 to 12–14 μm. Systems with such broadband radiation sources may become helpful in solving many applied problems of the atmospheric optics.

Lasers operating in the short-wave part of the near IR are now used to pump crystals, such as AgGaS₂ (transparency range of 0.47–13.0 μm) and Ag₃AsSe₃ (0.6–13.0 μm). However, these crystals have low nonlinear and thermal properties and a relatively low optical damage threshold, and, consequently, their frequency conversion efficiency is low as well.^{1,2} Not being biaxial, they have limited capabilities to frequency convert the radiation of the existing femtosecond lasers.

A low-abundance LiInSe₂ crystal of the mm2 point symmetry group, which falls in the family of ternary semiconductors of the I–II–VI₂ type, is among the promising crystals suitable for solution of the problem under consideration. Earlier Weise³ has studied the physical nature of different phases of the crystal; Greuling⁴ and Beister et al.,⁵ have considered

the transformation of the phases under pressure; Negran, Kasper, and Glass⁶ have found the pyroelectric and electrooptic coefficients; and Kamijoh and Kuriyama^{7,9} have determined the electric properties of this crystal.

The infrared and Raman frequencies were assessed by Eifler et al.⁸ Some papers^{6–10} are devoted to determination of the point symmetry group and the short-wave boundary of the transparency range (band gap),^{3,7,9–13} in particular, with the use of thin (300 μm) samples at the room and cryogenic (85 K) temperatures.¹² According to Refs. 7 and 9, the grown crystals have the *n*-type conductivity equal to 10¹¹–2.67 · 10¹¹ Ω·cm. According to recent data,^{5,12} the band gap ranges from 2.83 to 2.9 eV at the room temperature and amounts to 2.99 eV at the temperature of 80 K.

Depending on the crystal color, the short-wave boundary of the transparency range of real LiInSe₂ crystal samples lies within 0.438–0.775 μm interval, shifting toward longer waves as the crystal color varies from yellow to red. According to Refs. 3, 7, and 13, the color variations and the corresponding shift of the short-wave edge of the transparency range are attributed to lithium depletion and lead to appearance of inclusions of the second phase (LiIn₅Se₈).³ In Ref. 10 crystal color variations are explained by selenium depletion, and Ref. 13 points to both lithium and selenium depletion as a cause of this effect. In Refs. 14 and 15, the color of the LiInSe₂ crystal was varied from yellow to red due to optical illumination, which, in the authors' opinion, changed the charge state of point defects. The theoretical estimates of the quadratic nonlinear susceptibility coefficients have shown that they

should be close to the corresponding coefficients of the Ba₂NaNb₅O₁₅ crystal, that is, d_{31} and d_{32} should be roughly equal to 12–16 pm/V (Refs. 1 and 7).

Currently four research teams (Refs. 16, 17; 18–20; 21 and 22) continue investigation of the physical properties of the LiInSe₂ crystals. In Ref. 16 the second-order nonlinear susceptibility coefficients are determined to be $d_{31} = 10.6$ and $d_{32} = 6.3$ pm/V, and the obtained data on the band gap are close to those from Refs. 5 and 12. Kabanov et al.,²⁰ have found different values of the coefficients: $d_{31} = 12.2$ and $d_{32} = 10.8$ pm/V, and in Ref. 21 these coefficients are assumed equal to 20.0 and 17.0 pm/V for the general physics reasons. In addition, Ref. 16 reported on the study of some parameters of the second harmonic generator (SHG) of femtosecond radiation pulses in a BBO crystal traveling-wave oscillator, and SHG of TEA CO₂ lasers was addressed in Ref. 20. This paper presents the results of investigation of the optical properties, thermal conductivity, and the optical damage threshold of the LiInSe₂ crystal. These results were tested by SHG of mini-TEA and TEA CO₂ lasers as examples.

1. Linear optical properties

The investigations reported in this paper were carried out using a rich red colored sample of the LiInSe₂ crystal with the dimensions of 10.3×8×6.2 mm and orientation $\theta = 30^\circ$ in the XZ plane in the optical coordinate system (the angle is measured from the axis Z). The sample has been grown by the vertical Bridgeman technique with the temperature gradient of 20°C/cm in the crystallization zone with the translation rate of 6 mm/day. The transparency range of the sample was determined in the polarized light with the use of a Shimadzu UV-3101PC (working range of 0.3–3.2 μm) and a Specord 80M IR (2.5–25.0 μm) spectrophotometers. The dispersion properties and the Sellmeier coefficients $A, B, C, D,$ and E were found for the spectral region of 0.5–10.0 μm with the use of a GS-5 goniometer-spectrophotometer, and the lattice constants were estimated by the X-ray structure analysis technique using the CuK α radiation on a DRON-2 setup.²² The data on the linear optical properties are summarized in Table 1 and in Fig. 1.

Table 1. Summary data on the properties and parameters of LiInSe₂ single crystals

$\Delta\lambda, \mu\text{m}$	Sellmeier coefficients				$d_{ij}, \text{pm/V}$	Lattice constants, Å
	Coefficient	n_x	n_y	n_z		
0.59–13.5 (0%)	A	5.3726641	5.9556272	6.0160955	$d_{31} = \pm 12.6$ $d_{32} = \pm 6.3$	$a = 7.23; b = 8.45; c = 6.82.$ $X - b, Y - a, Z - c.$
	B	0.0861000	0.0950574	0.0885707		At $\lambda = 1.06 \mu\text{m}; 2V_z = 127.5^\circ;$
0.605–12.2 (10%)	C	-0.2148902	-0.2352307	-0.2398973		$n_x = 2.30; n_y = 2.34; n_z = 2.35.$
	D	274.89	489.27	493.78		At $\lambda = 9.55 \mu\text{m}$
	E	-86.338910	-357.58333	-368.73216		$2V_z = 125.5^\circ$

Notes. $\Delta\lambda$ is the spectral transparency range at the zero (0%) and 10% levels; the Sellmeier equation has the form $n^2 = A + C/(B - \lambda^2) + E/(D - \lambda^2)$; X, Y, and Z are optical axes; $a, b,$ and c are the lattice constants and the axes of the crystalline coordinate system; V_z is the angle between the axis Z and the optical axis; $n_x, n_y,$ and n_z are the principal refractive indices. In the optical coordinate system $n_x < n_y < n_z,$ and $n_y \approx n_z.$

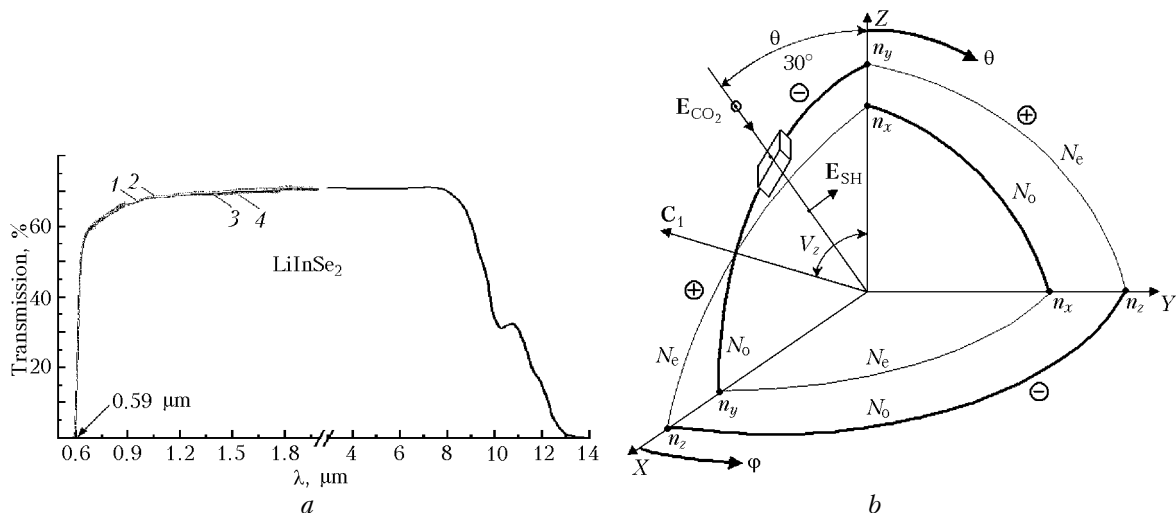


Fig. 1. Transmission spectrum of the LiInSe₂ crystal 6.2 mm thick for two points at the input surface (1, 2 and 3, 4) and waves of o - (1, 3) and e - (2, 4) polarization (a); double surface of refractive indices (b): C_1 is the optical axis, N_o and N_e are the refractive indices for the o - and e -waves; n_x, n_y, n_z are the refractive indices along the axes $x, y,$ and z ; \oplus and \ominus are the sectors, within which the crystal is positive or negative, V_z is the angle between the optical axis and the axis Z; ϕ and θ are the phase matching angles in the planes XY and XZ, YZ; E_{CO_2} and E_{SH} are the directions and polarization states of the pump and SH radiation.

The short-wave boundary of the transparency range at the zero measurement level is independent of the incident light polarization. In the adjacent part of the transparency range $\leq 0.9 \mu\text{m}$, the scattering of radiation by the microinclusions contributes markedly (up to 30%) to the radiation extinction. Variations of transparency at different points of illumination of the input crystal surface did not exceed 2%. The optical loss coefficient in the region of maximum transparency was less than 0.1 cm^{-1} , and at the wavelengths of 9.55 and $10.6 \mu\text{m}$ it was 0.55 and 1.2 cm^{-1} , respectively. Slight variations in the short-wave part of the transparency curve are caused by the replacement of optical elements in the Shimadzu UV-3101PC spectrophotometer used.

2. Thermal conductivity

The thermal conductivity and thermal capacity are important characteristics of nonlinear crystals, because they determine the processes of formation of the temperature gradient and thermal lenses, which cause violation of the phase matching conditions and restrict the pump power owing to breakdown of the output surface of the crystal. The data on the thermal conductivity for LiInSe₂ crystals can be found in Ref. 23; in particular, at the room temperature it is $0.34 \text{ J}/(\text{g}\cdot\text{K})$. For a comparison, the thermal capacity of Te, CdGeAs₂, ZnGeP₂, Tl₃AsSe₃, AgGaSe₂, GaSe, and CdSe is, respectively, 0.21 , 0.3 , 0.463 , 0.19 , 0.3 , 0.35 , and $0.0875 \text{ (LN) J}/(\text{g}\cdot\text{K})$.

The thermal conductivity was measured by the method of dynamic calorimetry with an IT- λ -400 meter of thermal conductivity (measurement accuracy $\pm 10\%$). The meter was calibrated with the aid of sample measures of thermal conductivity made of fused quartz and copper. The control measurements were conducted using an AgGaS₂ crystal with the well-known thermal conductivity of $0.015 \text{ W}/\text{cm}^2\cdot\text{K}$ (Ref. 24). The fact that the crystal cross section area differed from the standard measurement area of the IT- λ -400 meter and its influence on the measurement accuracy were taken into account analytically. The equation for the total heat resistance of the gap between the heat source and the receiving rod was considered by analogy with the electric resistance of two parallel circuits, and the thermal conductivity of air at 20°C was taken equal to $0.00026 \text{ W}/\text{cm}^2\cdot\text{K}$. The additional measurement error did not exceed $\pm 2\%$. The measured thermal conductivity was $(0.014 \pm \pm 0.002) \text{ W}/(\text{cm}^2\cdot\text{K})$, which is close to the thermal conductivity of the AgGaS₂ crystal. Despite the thermal conductivity of the LiInSe₂ crystals is 25.7 times lower than that of the ZnGeP₂ crystals, it

sevenfold exceeds the thermal conductivity of Te crystals, fourfold that of the Tl₃AsSe₃ crystals, and is 1.3 times higher than that of the AgGaSe₂ crystals.

3. Optical damage threshold

The maximum efficiency of the frequency conversion is determined by the value of the product $M \times I_d$, where I_d is the optical damage threshold of the crystal (with the allowance made for the effect of the thermal lens), and $M = d_{\text{eff}}^2/n^3$ is the figure of merit of a crystal, which is proportional to the frequency conversion efficiency, d_{eff} is the effective second-order nonlinear susceptibility coefficient, n is the mean value of the refractive index for the interacting wavelengths. The optical damage threshold of the LiInSe₂ crystals was determined with the help of a TEA CO₂ laser operated at the 9P(20) line (wavelength of $9.55 \mu\text{m}$) in comparison with some other nonlinear crystals under the identical experimental conditions and after the identical mechanical treatment of the crystals. The measurement procedure is described in Ref. 4. The laser emitted pulses of $(30 \pm 2)\text{-ns}$ duration (FWHM) with the energy of 560 mJ in the TEM₀₀ mode with about 90% of the total pulse energy contained in the leading peak.

According to the repeated measurements, the optical damage threshold was found to be $(248 \pm 16) \text{ MW}/\text{cm}^2$, which is $1.6\text{--}1.8$ times higher than that of the widely used crystals, such as CdGeAs₂ (157 ± 13), ZnGeP₂ (142 ± 9), AgGaSe₂ (139 ± 6), AgGaS₂ (149 ± 6) MW/cm^2 , and by 9% higher than optical damage threshold of the new AgGaGeS₄ crystal (230 ± 9) MW/cm^2 . So, that high damage threshold compensates for the advantages of these crystals in the nonlinear properties.

4. Phase matching conditions

The analysis of the possibilities of meeting the phase matching conditions shows that SHG can be obtained in the LiInSe₂ crystal in a wide spectral range from 1.84 to $10 \mu\text{m}$ and even up to $11.87 \mu\text{m}$ on the assumption of correctness of the Sellmeier equations for long waves. For illustration, Table 2 gives the diagrams of transitions between the stereographic projections of the phase matching directions for SHG in the crystal volume.

The types of the stereographic projections in accordance with the commonly accepted classification²⁵ are given in the upper row of the Table 2, and the type of interaction and the wavelengths, at which the transition from one type of projection to another occurs, are given in the second row.

Table 2. Diagrams of transitions between stereographic projections of phase matching directions for SHG in LiInSe₂

Type																					
sff ssf		1841.5		2064.2			2628.0			3051.1			7107.5			8278.5		10523		11871	

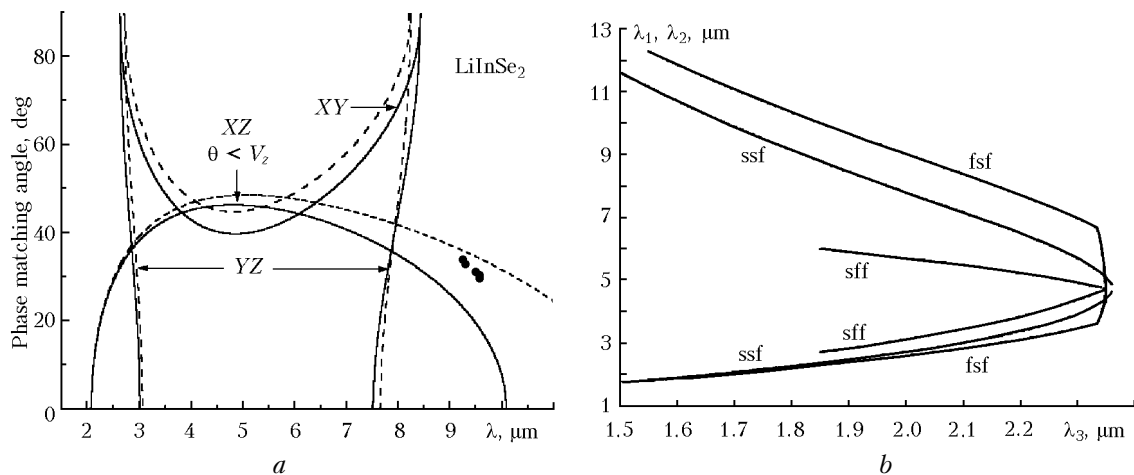


Fig. 2. Phase matching curves for SHG in the principal planes of the LiInSe₂ crystal according to data of this work (solid lines) and Ref. 16 (dashed lines); experimental data (dots) (a). The dependence of the wavelengths λ_1 and λ_2 of femtosecond pump pulses, for which sum frequency generation with pulse compression takes place in the plane XY, on the wavelength λ_3 of the sum frequency radiation (b).

The second harmonic generation is also possible at interactions in all the three principal planes of the crystal (Fig. 2a). In the XY plane, SHG occurs by the sff and fsf types of interaction in the spectral range from 2.62 to 8.45 μm with $d_{\text{eff}} = d_{32} \sin^2 \varphi + d_{31} \cos^2 \varphi$ at the angle φ varying within 0–90°. The same types of interaction take place in the YZ plane within roughly the same spectral range with $d_{\text{eff}} = d_{32} \sin \theta$ at the angle θ varying within 0–90°, and in the XZ plane the interaction of the ssf type with $d_{\text{eff}} = d_{31} \sin \theta$ occurs at $\theta < V_z$. At $\theta > V_z$ the birefringence proves insufficient for realization of SHG by the interaction of the sff and fsf types with $d_{\text{eff}} = d_{31} \sin \theta$.

It can be seen from Fig. 2a that the Sellmeier equation obtained in this paper and the Sellmeier equation from Ref. 16 give quite close results, except for the long-wave part of the phase matching curves in the XZ plane. The experimental data on SHG of the CO₂ laser are closest to the estimates by the Sellmeier equations obtained in Ref. 22.

It is important that, due to high birefringence, the parametric generation of light in the LiInSe₂ crystals takes place at pumping by radiation of all solid-state lasers operating in the near IR region, at least, within the spectral range, for which the Sellmeier equations are determined.

The group-velocity matching in the direction of phase matching, as a necessary condition for SHG of femtosecond pulses with preservation of their time shape, is fulfilled for the spectral region of 3.05–7.11 μm . One of the possible modes of frequency conversion of femtosecond pulses is the mode, in which the group-velocity mismatches for two pairs of interacting waves have the opposite signs, that is, $(1/v_1 - 1/v_3) = -(1/v_2 - 1/v_3)$. With the proper choice of the delay between pulses at the crystal input, the pulse intensity, and the crystal length, it is possible to obtain frequency conversion with compression of the pulse duration.

For example, Fig. 2b depicts the dependences of the wavelengths λ_1 and λ_2 of the mixed radiation, for which sum frequency generation with pulse compression takes place in the XY plane, on the wavelength λ_3 of the generated radiation. It should be noted that this mode can be obtained for all types of interaction. According to the estimates, one of the realizations of this mode is conversion (at sum frequency generation) of 100 fs pulses at the wavelengths $\lambda_1 = 11.598$ and $\lambda_2 = 1.7228$ μm . At the radiation intensity of 10 GW/cm² and the crystal length of 16 mm, the energy conversion efficiency is 28%. But the pulse duration in this case decreases 10 times, and the peak power increases 4 times (the power conversion efficiency is about 200%).

5. Experiment

The estimated potential efficiency of SHG of CO₂ laser in LiInSe₂ as compared to that of the widely used ZnGeP₂, AgGaS₂, LiInS₂ crystals and some other rarely used and new crystals is given in Table 3. To estimate the SHG efficiency in the XZ plane, we used the experimentally determined value of the phase matching angle equal to 30° (see below), rather than the estimate by the Sellmeier equations (18°). The plane and the type of interaction are given in parenthesis near d_{eff} . Because the phase matching conditions cannot be fulfilled in LiInS₂ for SHG of the CO₂ laser, the estimated data for SHG of the CO laser are presented.

Thus, the potential efficiency of SHG of CO₂ lasers for some crystals have been determined with the allowance for the obtained data on the optical damage threshold, phase matching conditions, and from the nonlinear properties of the LiInSe₂ crystals. In addition, it was assumed that the optical losses of different crystals are close at the wavelengths of the 9- μm emission band of the CO₂ laser.

Table 3. Parameters and potential efficiency of nonlinear crystals at SHG of CO₂ laser radiation (9P(20) line at the wavelength of 9.55 μm)

Crystal	$\Delta\lambda$, μm	n	B	d_{ij} , pm/V	$\theta(\varphi)$, deg	d_{eff} (type of interaction)	M_{sh} , (pm/V) ²	M' , %	I_d , rel. units	$M' \times I_d$, %
LiInSe ₂	0.59–13.5	2.241	0.044	$d_{31}=12.2$	–	$d_{31}\cos^2\varphi+d_{32}\sin^2\varphi$ (XY, sff and fsf)	–	–	1.7	–
				$d_{32}=10.8$	–	$d_{32}\sin\theta$ (YZ, sff and fsf)	–	–	–	–
					30	$d_{31}\sin\theta$ (XZ, $\theta < V_z$, sff)	6.1	7	–	11.9
LiInS ₂ (CO laser)	0.34–13.2	2.156	0.053	$d_{31}=6.2$	63	$d_{31}\cos^2\varphi+d_{32}\sin^2\varphi$ (XY, sff and fsf)	3.1	3.5	1.7	6.0
				$d_{32}=5.4$	–	$d_{32}\sin\theta$ (YZ, sff and fsf)	–	–	–	–
					40.5	$d_{31}\sin\theta$ (XZ, sff)	4.0	1.6	–	2.8
ZnGeP ₂	0.7–12.0	3.10	0.04	$d_{36}=75$	68.6	$d_{36}\sin 2\theta\cos 2\varphi$ (I)	87.2	100	1	100
AgGaS ₂	0.47–13.0	2.36	0.053	$d_{36}=11.7$	58	$d_{36}\sin\theta\sin 2\varphi$ (I)	7.5	8.6	1.3	11.2
HgGa ₂ S ₄	0.49–15.5	2.362	0.045	$d_{36}=35.2$	72.6	$d_{36}\sin\theta\sin 2\varphi+d_{31}\sin\theta\cos 2\varphi$ (I)	95.3	109	2.2	240.3
				$d_{31}=11.7$	–	$d_{31}\sin 2\theta\sin 2\varphi-d_{36}\sin 2\theta\cos 2\varphi$ (II)	12.4	13.4	–	29.4
Hg _{1-x} Cd _x Ga ₂ S ₄ ($x = 0.1$)	0.46–15.0	2.301	0.024	$d_{36}=34.1$	90	$d_{36}\sin\theta\sin 2\varphi+d_{31}\sin\theta\cos 2\varphi$ (I)	106.4	122	1.9	232
				$d_{31}=11.3$	–	$d_{31}\sin 2\theta\sin 2\varphi-d_{36}\sin 2\theta\cos 2\varphi$ (II)	–	–	–	–
AgGaGe _x S _{2(1+x)} ($x = 1$)	0.45–14.5	2.246	0.057	$d_{31}=8$	–	$d_{32}\cos^2\varphi+d_{31}\sin^2\varphi$ (XY, sff)	–	–	1.6	–
				$d_{32}=13$	61.5	$d_{32}\sin\theta$ (YZ, sff)	11.8	13.5	–	21.6
					56.5	$d_{31}\sin\theta$ (XZ, sff)	3.2	3.7	–	5.9

Notes. $\Delta\lambda$ is the transparency range at the zero level; n is the refractive index at the wavelength of 9.55 μm; B is the maximum birefringence; d_{ij} are the coefficients of the nonlinear susceptibility tensor; M_{sh} and M' are the absolute and normalized values of the figure of merit for SHG of radiation with the wavelength of 9.55 μm; I_d is the optical damage threshold.

It follows from Table 3 that the efficiency of SHG of CO₂ laser in LiInSe₂ crystals is much lower than that in the HgGa₂S₄, Hg_{0.9}Cd_{0.1}Ga₂S₄, and ZnGeP₂ crystals, but quite comparable with the efficiency of the AgGaS₂ crystals and it is twice as high as that of LiInS₂.

Second harmonic generation was obtained for all lines of the 9-μm band of the TEA and mini-TEA CO₂ lasers^{2,20} at the phase matching angles different by 10–12° from the values calculated by the Sellmeier equations and different by 3–4° from the estimates obtained using the data from Ref. 16 (Fig. 2a). The dependence of the SH energy on the angular detuning from the phase matching direction and on the wavelength is exemplified in Figs. 3a and b.

The efficiency of frequency doubling for the 9R(22) line of the CO₂ laser with the wavelength of 9.26 μm is maximum and equal to (4.3 ± 0.2)%, which is 8.2 times lower than that of the HgGa₂S₄ crystals,²⁰ but agrees well with the expected result. The decrease of the SHG efficiency for the radiation with shorter wavelengths is caused by the decrease in the energy characteristics of the CO₂ laser radiation, and a twofold decrease at the longer wavelengths, which is always observed in the region of 9.3–9.6 μm, is due to the increasing optical loss in the crystal, on the one hand, and the increasing radiation power, on the other hand.

Thus, the external efficiency of SHG of the 9P(20) line with the wavelength of 9.55 μm (earlier this line was used as a reference one for comparing the SHG efficiencies of different crystals²⁰) for the peak power was only (2.6 ± 0.1)%, and for energy it was (1.50 ± 0.04)% at the pump intensity of (38.5 ± 0.4) MW/cm². This intensity amounts to only 16% of the damage threshold of the crystal to exclude

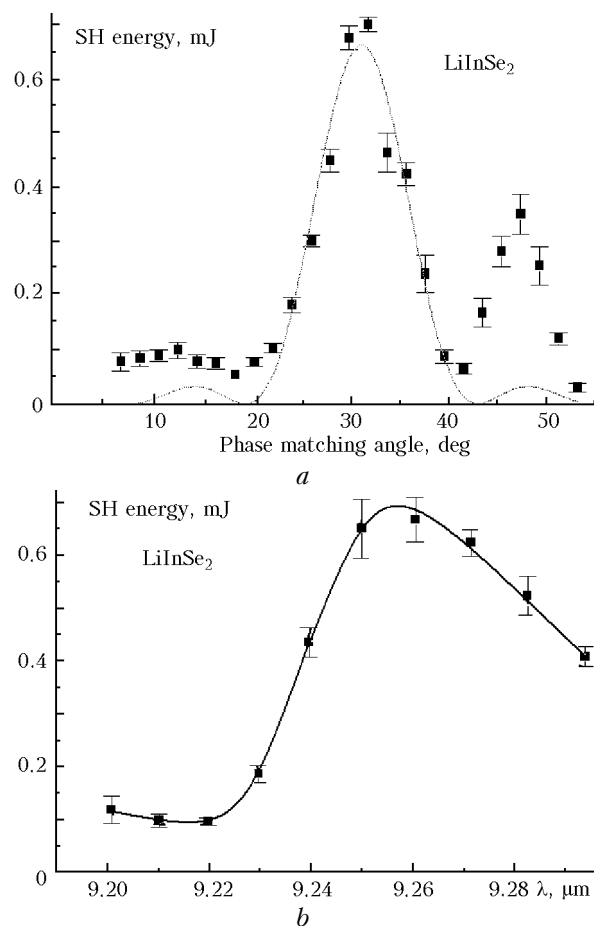


Fig. 3. Energy of the second harmonic of the 9R(22) line of the CO₂ laser at the room temperature versus angular detuning from the phase matching direction (the curve is an estimation result) (a) and the pump wavelength (the curve is approximation by least-squares method) (b).

the effect of thermal processes on the measurement results. The maximum SH energy in this case was (7.2 ± 0.1) mJ, and the peak power was (45.6 ± 0.21) kW/cm².

Conclusion

The spectral transparency range and the high birefringence of the biaxial LiInSe₂ crystals allow one to realize the SHG of all widely used mid-IR lasers, including SHG of the CO₂ laser. However, in the combination of physical properties such generators are inferior to those based on the ZnGeP₂ and HgGa₂S₄ crystals (8.2 times) and Hg_{0.9}Cd_{0.1}Ga₂S₄ crystals, as well as, consequently, CdGeAs₂ crystals. Their efficiency is identical to that of the AgGaS₂ crystals and twice as high as the efficiency of LiInS₂ crystals. The advantage of the LiInSe₂ crystals is the possibility of creating mid-IR parametric light oscillators pumped by radiation of near-IR solid-state lasers, in particular, Nd:YAG lasers, with more than doubled efficiency as compared to that of AgGaS₂ and LiInS₂ crystals used. It is also worth noting the potential advantage of the LiInSe₂ crystals in frequency conversion of femtosecond pulses over all known crystals both in the mid IR region and in direct conversion of radiation of femtosecond Ti:sapphire and Cr:forsterite lasers into the mid IR region.

References

1. G.G. Gurzadyan, V.G. Dmitriev, and D.N. Nikogosyan, *Handbook on Nonlinear Optical Crystals* (Springer Verlag, New York–Berlin, 1999), 413 pp.
2. Yu.M. Andreev, V.V. Badikov, V.G. Voevodin, L.G. Geiko, P.P. Geiko, M.V. Ivashchenko, A.I. Karapuzikov, and I.V. Sherstov, *Quant. Electron.* **31**, No. 12, 1075–1078 (2001).
3. S. Weise, "Zuchtung und charakterisierung von kristallen im system Li₂Se–In₂Se₃," Author's Abstract of Diss. (University Frieburg, 2001), 4 pp.
4. B. Greuling, *Cryst. Res. Technol.* **22**, No. 2, K27–K29 (1987).
5. H.J. Beister, S. Ves, W. Honle, K. Syassen, and G. Kuhn, *Phys. Rev. B* **43**, No. 12, 9635–9642 (1991).
6. T.J. Negran, H.M. Kasper, and A.M. Glass, *Mater. Res. Bull.* **8**, No. 6, 743–747 (1973).
7. T. Kamijoh and K. Kuriyama, *J. Crystal Growth* **51**, No. 1, 6–10 (1981).
8. A. Eifler, V. Reide, S. Wenger, S. Weise, E. Nowak, D. Sprinz, G. Lippold, and W. Grill, in: *Proc. of 10th Int. Conf. on Ternary and Multinary Compounds* (Stuttgart, 1995), pp. 359–362.
9. T. Kamijoh and K. Kuriyama, *J. Appl. Phys.* **52**, No. 2, 1102–1103 (1981).
10. T. Kamijoh and K. Kuriyama, *J. Crystal Growth* **46**, No. 6, 801–803 (1981).
11. K. Kuriyama, Y. Igarashi, F. Nakamura, and A. Okada, *Appl. Phys. Lett.* **48**, No. 18, 1199–1201 (1986).
12. A. Eifler, V. Reide, S. Wenger, S. Weise, E. Nowak, and V. Kramer, in: *Proc. of 10th Int. Conf. on Ternary and Multinary Compounds* (Stuttgart, 1995), pp. 363–366.
13. C.J. Smith and C.W. Lowe, *J. Appl. Phys.* **66**, No. 10, 5102–5104 (1989).
14. W. Horig, H. Neuman, and G. Kuhn, *Phys. Stat. Sol. (b)* **121**, K55–K58 (1984).
15. L. Isaenko, A. Yeliseev, J.J. Zondy, G. Knippels, I. Thenot, and S. Lobanov, *Optoelectron. Rev.* **9**, No. 2, 135–142 (2001).
16. L. Isaenko, A. Yeliseev, S. Lobanov, V. Petrov, F. Rotermund, G. Sleky, and J.J. Zondy, *J. Appl. Phys.* **91**, No. 12, 9475–9480 (2002).
17. L.I. Isaenko, "Performing of new nonlinear LiInS₂ and LiInSe₂ crystals for estimation of their application outlooks," ISTC Project 2006 (2003), 3 pp.
18. Yu.M. Andreev, V.V. Badikov, P.P. Geiko, L.G. Geiko, V.V. Efimenko, T.D. Efimenko, M.V. Ivashchenko, A.I. Karapuzikov, V.L. Panyutin, and I.V. Sherstov, in: *Proc. of III Int. Symp. on Monitoring and Rehabilitation of the Environment* (Tomsk, 2002), pp. 61–62.
19. Yu.M. Andreev, V.V. Badikov, P.P. Geiko, V.V. Efimenko, T.D. Efimenko, M.V. Ivaschenko, A.I. Karapuzikov, V.L. Panyutin, and I.V. Sherstov, in: *Proc. of the VI Russian-Korean International Symposium on Science and Technology (KORUS-2002)* (Novosibirsk, 2002), Vol. 1, pp. 303–306.
20. M.V. Kabanov, Yu.M. Andreev, V.V. Badikov, and P.P. Geiko, *Izv. Vyssh. Uchebn. Zaved., Fizika* **46**, No. 8, 84–94 (2003).
21. V.V. Badikov, V.I. Chizikov, V.V. Efimenko, V.L. Panyutin, G.S. Shevyrdyaeva, and S.I. Scherbakov, *Opt. Mater.* **23**, 575–581 (2003).
22. V.V. Popov, H.C. Trocenko, and V.V. Atuchin, *J. Crystal Growth* (in press) and *Int. Conf. on Materials for Advanced Technol. (ICMAT 2003)* (Singapore, 2003), Rep. H13-3.
23. G. Kuhn, E. Piri, H. Neuman, and E. Nowak, *Cryst. Res. Technol.* **22**, No. 2, 265–269 (1987).
24. J.D. Beasley, *Appl. Opt.* **33**, No. 6, 1000–1003 (1994).
25. S.G. Grechin, S.C. Grechin, and V.G. Dmitriev, *Quant. Electron.* **30**, No. 5, 377–386 (2000).